PNAS RESEARCH ARTICLE | IMMUNOLOGY AND INFLAMMATION

The pyruvate–GPR31 axis promotes transepithelial dendrite formation in human intestinal dendritic cells

Eri Oguro-Igashira[a,b,c], Mari Murakami[a,b], Ryota Mori[d], Ryuichi Kuwahara[e], Takako Kihara[f], Masaharu Kohara[g], Makoto Fujiwara[h], Daisuke Motooka[b,i,j], Daisuke Okuzaki[b,i,j,k,l], Mitsuru Arase[a,b], Hironobu Toyota[a], Siyun Peng[a,b], Takayuki Ogino[d], Yasuji Kitabatake[h], Eiichi Morii[g], Seiichi Hirota[f], Hiroki Ikeuchi[e], Eiji Umemoto[m], Atsushi Kumanogoh[c,j,k,l,n], and Kiyoshi Takeda[a,b,j,k,1]

Affiliations are included on p. 11.

Edited by Jason Cyster, HHMI, University of California San Francisco, San Francisco, CA; received October 26, 2023; accepted August 30, 2024

The intestinal lumen is rich in gut microbial metabolites that serve as signaling molecules for gut immune cells. G-protein-coupled receptors (GPCRs) sense metabolites and can act as key mediators that translate gut luminal signals into host immune responses. However, the impacts of gut microbe–GPCR interactions on human physiology have not been fully elucidated. Here, we show that GPR31, which is activated by the gut bacterial metabolite pyruvate, is specifically expressed on type 1 conventional dendritic cells (cDC1s) in the lamina propria of the human intestine. Using human induced pluripotent stem cell-derived cDC1s and a monolayer human gut organoid coculture system, we show that cDC1s extend their dendrites toward pyruvate on the luminal side, forming transepithelial dendrites (TED). Accordingly, GPR31 activation via pyruvate enhances the fundamental function of cDC1 by allowing efficient uptake of gut luminal antigens, such as dietary compounds and bacterial particles through TED formation. Our results highlight the role of GPCRs in tuning the human gut immune system according to local metabolic cues.

G protein-coupled receptors | GPR31 | dendritic cell | transepithelial dendrite formation | antigen recognition

Significance

Transepithelial dendrite (TED) formation of dendritic cells is an important biological process responsible for antigen sampling and immune surveillance in the gut, playing a crucial role in maintaining gut homeostasis. However, factors driving TED formation in humans are poorly understood due to difficulties in human cell-based experiments. Here, we use state-of-the-art technology to demonstrate that an environmental cue controls the formation of TED in human type 1 conventional dendritic cell (cDC1). This process is mediated by GPR31, which is found to be highly expressed in intestinal cDC1, and its activation promotes the uptake of gut luminal antigens. These results may provide potential targets for clinical applications, such as protection from intestinal infections and improvements in mucosal vaccine efficacy.

The human gut microbiota is composed of ~38 trillion microbes (1), which produce various metabolites that affect host health (2–4). G-protein-coupled receptors (GPCRs), the largest family of human membrane proteins, play a central role in recognizing these metabolites, which play important roles in the maintenance of gut and overall host health by serving as signaling molecules for immune cells, epithelial cells, and neurons (5, 6). Although many GPCRs remain uncharacterized, recent technological advances—including functional metagenomics (7), bioinformatics in combination with synthetic biology (8), high-throughput functional profiling approach (9), and multiplexed bioactivity screening (10)—have led to the identification of many novel ligands and functions of GPCRs. For example, GPR56 and GPR97 are activated by the essential amino acid L-phenylalanine, which is produced by certain *Bacteroides* strains (9). Because intestinal metabolites are complex and diverse, there is a need for further exploration of interactions between metabolites and GPCRs in the gut. Moreover, the expression levels of GPCRs vary among cell types, implying that metabolites act on specific cell types and influence their functional characteristics. Intestinal mononuclear phagocytes (MNPs), including monocytes, macrophages, and dendritic cells (DCs) (11), play key roles in maintaining gut homeostasis through antigen recognition and presentation to adaptive immune cells. Therefore, the identification of cell type–specific GPCRs in human intestinal MNP subsets and elucidation of mechanisms by which metabolic niches influence function are important areas of research to understand the mechanisms of gut homeostasis; exploration of these areas may provide potential therapeutic targets for gastrointestinal and immune diseases.

Although single-cell analysis of human gastrointestinal cell populations enables a comprehensive understanding of the gut immune system, it generally does not provide sufficient resolution for MNPs, which are substantially less abundant than stromal cells, epithelial cells, and lymphocytes (12). Publicly accessible single-cell RNA sequencing (scRNA-seq) datasets focused on human intestinal MNPs are limited and mainly targeted to the human colon (13–15). Here, we utilized a single-cell approach that exclusively targeted human small intestinal MNPs to examine subset-specific expression of GPCRs with unknown endogenous ligands. Among GPCR family members, GPR31 was specifically expressed on human type 1 conventional dendritic cells (cDC1s), with particularly high expression in small intestinal cDC1s. In mice, CX3CR1^{+} intestinal myeloid cells protrude dendrites across epithelial barriers for antigen uptake (16). We previously showed

Author contributions: E.O.-I., M.M., and K.T. designed research; E.O.-I., M.M., R.M., R.K., T.K., M.K., M.F., H.T., S.P., T.O., Y.K., E.M., S.H., H.I., E.U., and A.K. performed research; E.O.-I., D.M., D.O., and M.A. analyzed data; and E.O.-I., M.M., and K.T. wrote the paper.

The authors declare no competing interest.

This article is a PNAS Direct Submission.

[1]To whom correspondence may be addressed. Email: ktakeda@ongene.med.osaka-u.ac.jp.

This article contains supporting information online at https://www.pnas.org/lookup/suppl/doi:10.1073/pnas.2318767121/-/DCSupplemental.

Published October 21, 2024.

that pyruvate (PA) and lactate (LA)—metabolites of gut commensal microbes—promote dendrite protrusion from CX3CR1$^+$ intestinal myeloid cells via GPR31 in mice (17). It is important to determine whether this function is preserved in humans and to identify its effects in human physiology. In this study, we used induced pluripotent stem cell (iPSC) technology and a human gut organoid system to demonstrate that the PA–GPR31–dendrite protrusion axis, mediated by changes in cytoskeletal conformation, is broadly conserved across species and cell types. These findings provide insights concerning the mechanism by which gut microbiota regulate transepithelial dendrite (TED) formation of human cDC1s.

Results

GPR31 Is Specifically Expressed on cDC1s in Human Intestinal MNPs. To systematically evaluate human intestinal MNPs, we performed scRNA-seq analysis (10× Chromium) on CD3$^-$CD19$^-$CD20$^-$CD56$^-$EpCAM$^-$CD45$^+$HLA-DR$^+$ live cells in lamina propria isolated from the unaffected mucosa of the human ileum (n = 4) (*SI Appendix*, Fig. S1*A* and Table S1). *CD3E*$^+$ T cells (clusters 14, 15), *CD79A*$^+$ B cells (clusters 16 to 18), *COL3A1*$^+$ stromal cells (cluster 17), and *CPA3*$^+$ mast cells (cluster 19) were excluded prior to analysis (*SI Appendix*, Fig. S1*B*). The analyzed data consisted of 10,234 MNPs across 13 clusters (Fig. 1 *A*–*C* and *SI Appendix*, Fig. S2 *A* and *B*). MNPs were mainly subdivided into two main lineages, monocyte-macrophage lineage (clusters 1 to 5; expressing *CD14*) and DC lineage (clusters 6 to 12; expressing *FLT3*) (Fig. 1*C*). By comparing the gene expression patterns of each cluster to the previously reported transcriptional signatures of each cell type, cells were classified into 9 cell types (Fig. 1*B* and *SI Appendix*, Fig. S2 *A* and *B*) (14, 18–23).

GPCRs with unknown ligands are potential targets in efforts to identify metabolites functioning as novel ligands (26). Therefore, the expression levels of genes encoding GPCRs with unknown ligands in human intestinal MNPs were surveyed using scRNA-seq data. Although most GPCR-encoding genes were ubiquitously expressed on cells in various clusters, *GPR31* was specifically expressed on cDC1s (cluster 6) (Fig. 1 *D* and *E*). This result was confirmed by targeted scRNA-seq analysis for more sensitive detection of targeted transcripts (BD Rhapsody) and evaluation of each MNP subset by bulk RNA-seq analysis, both of which showed specific expression of *GPR31* to cDC1s (*SI Appendix*, Fig. S3 *A*–*D*). Analysis using a publicly accessible multitissue scRNA-seq dataset of human immune cells (including innate and adaptive immune cells) showed that *GPR31* was specifically expressed in cDC1s in the jejunum and other organs (*SI Appendix*, Fig. S4) (25); it displayed particularly high expression in the intestinal lamina propria (Fig. 1*F*). These results led us to assume that *GPR31* specifically influences human intestinal cDC1 activity in response to gut luminal metabolites.

Human Intestinal cDC1 Activation by PA Led to Dendrite Elongation. Because *GPR31* was expressed in 35% of cDC1s (Fig. 2*A*), we investigated whether GPR31 expression confers specific functional characteristics to these cDC1s. Pathway analysis of scRNA-seq data showed that *GPR31*$^+$ cDC1s were enriched in Gene Ontology (GO) terms related to antigen processing and presentation, as well as interferon-γ-mediated signaling, compared with *GPR31*$^-$ cDC1s (Fig. 2 *B* and *C*). These results suggest that GPR31 expression on cDC1s could enhance their antigen processing and presentation capacities.

GPR31 is reportedly activated by the gut bacterial metabolites PA and LA (17), as well as 12(S)-hydroxyeicosatetraenoic acid [12(S)-HETE], a 12-lipoxygenase metabolite of arachidonic acid (27). Therefore, we investigated whether cDC1s could be activated by these metabolites. Because commercially available antibodies we tested failed to specifically detect human GPR31, cDC1s isolated from resected human gut samples using an antibody to XCR1, a representative marker of cDC1s, were used for subsequent analyses (Fig. 1*C* and *SI Appendix*, Fig. S5*A*); the isolated cDC1s were stimulated with PA, LA, and 12(S)-HETE. Consistent with the results of scRNA-seq analysis, XCR1$^+$ conventional dendritic cells (cDCs) in human intestinal lamina propria showed significantly higher *GPR31* expression, compared with XCR1$^-$ cDCs (*SI Appendix*, Fig. S5*B*). To investigate stimulation-induced transcriptional changes in human intestinal cDC1s, bulk RNA-seq of isolated human intestinal cDC1s was performed after stimulation with PA, LA, or 12(S)-HETE. Differentially expressed genes that were up-regulated upon stimulation included genes associated with dendritic membranes and filopodia, such as *KITLG*, *MPP2, ERMN*, *KCNB1*, and *TTC8* (Fig. 2*D* and *SI Appendix*, Fig. S5*C*). Filopodia reportedly function as phagocytic tentacles, pulling captured antigens toward the cell for phagocytosis; this could be a mechanism to enhance phagocytic uptake (28). The results concerning differentially expressed genes suggest that human intestinal cDC1s are activated by the bacterial metabolites, which can lead to morphological changes in cDC1s. Indeed, the percentage of dendrite-elongating cDC1s was significantly increased after PA stimulation in vitro (Fig. 2*E*). This result was further confirmed in cDC1s isolated from gut-associated lymphoid tissue (GALT)-free lamina propria (*SI Appendix*, Fig. S5*D*). In contrast, PA stimulation had no significant impact on general activation markers of DCs (CD40, CD80, CD83, and CD86) (29–31), implicating that PA induces morphological changes in cDC1s without triggering their general activation (*SI Appendix*, Fig. S5*E*). To investigate the involvement of GPR31, *GPR31* expression in human intestinal cDC1s was knocked down by small interfering RNA (siRNA). PA-induced dendritic elongation was canceled by *GPR31* knockdown (*SI Appendix*, Fig. S5*F*). These results indicated that PA promotes dendrite extension of human intestinal cDC1s in a manner that is mediated by GPR31.

PA Stimulation Caused GPR31-Dependent Dendrite Protrusion in Human cDC1s. To investigate whether the PA–GPR31 axis mediates dendrite protrusion of cDC1s, cDC1s with drug-inducible *GPR31* were generated using human iPSCs. First, a vector (PB-TAG-ERN) containing the human *GPR31* sequence was constructed using the *piggyBac* transposon vector system (32). This vector was designed to express *GPR31* in a doxycycline (DOX)-dependent manner and simultaneously express green fluorescent protein (GFP). PB-TAG-ERN containing the human *GPR31* sequence was cotransfected into human iPSCs along with *piggyBac* transposase (PBase) (Fig. 3*A*). DOX-stimulated iPSCs displayed efficient (~95%) induction of GFP and high expression of *GPR31* (*SI Appendix*, Fig. S6 *A* and *B*). Subsequently, cDC1 differentiation was induced in *GPR31*-transduced iPSCs by cytokine cocktail stimulation, as previously reported (Fig. 3*B*) (33, 34). To purify iPSC-derived cDC1s, CD11c$^+$XCR1$^+$ live cells were isolated by a flow cytometer and subsequently used for the study (*SI Appendix*, Fig. S6*C*). iPSC-derived cDC1s exhibited DC-like cellular morphology with dendrites (Fig. 3*C* and *SI Appendix*, Fig. S6*D*) and expressed *XCR1* and *GPR31* (*SI Appendix*, Fig. S6 *E* and *F*). Furthermore, the pattern of cell surface marker expression on iPSC-derived cDC1s was consistent with a previously reported cDC1 pattern; XCR1$^+$, CD11c$^+$, CD141$^+$, CD1c$^-$, and CD123$^-$ (*SI Appendix*, Fig. S6 *G* and *H*) (35). Stimulation with lipopolysaccharide (LPS) increased surface expression of activation

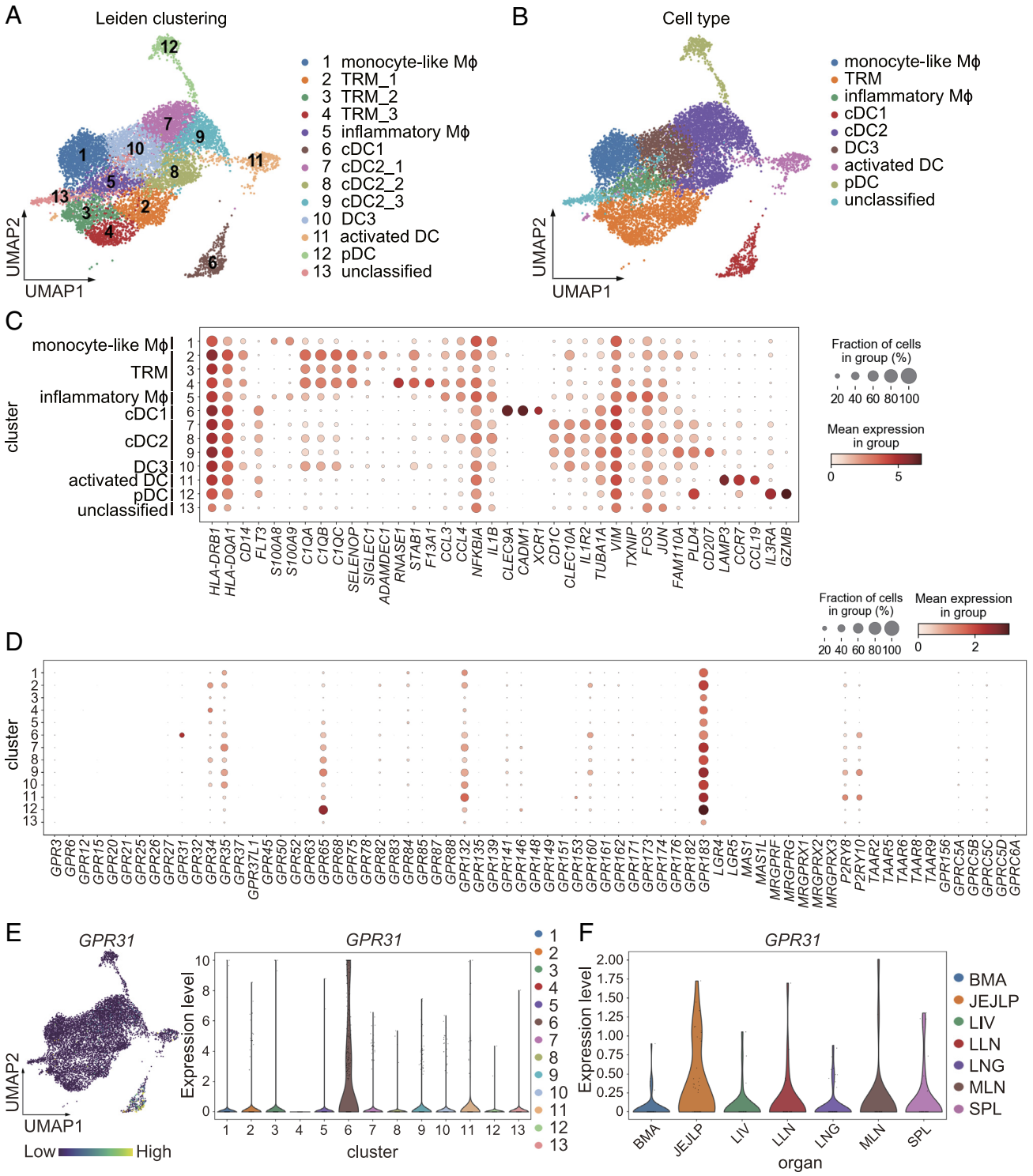

Fig. 1. scRNA-seq analysis profiles of cell type–specific GPCRs in human intestinal MNPs. (*A*–*E*) scRNA-seq analysis of 10,234 MNPs from human ileal lamina propria (n = 4). (*A*) UMAP plot of Leiden clustering. TRM, tissue-resident macrophage; cDC2, type 2 conventional dendritic cell; pDC, plasmacytoid dendritic cell. (*B*) UMAP plot of cell type. (*C*) Dot plot heatmap showing expression of representative marker genes. (*D*) Dot plot of gene expression for orphan GPCRs (24). (*E*) *Left*: *GPR31* expression on the UMAP plot, represented as a heatmap. *Right*: Violin plot of *GPR31* expression in each cluster. (*F*) Reanalysis of publicly accessible multitissue scRNA-seq dataset of human myeloid cells (25). Violin plot of *GPR31* expression in cDC1 subsets of each organ. BMA, bone marrow; JEJLP, jejunal lamina propria; LIV, liver; LLN, lung-draining lymph nodes; LNG, lung; MLN, mesenteric lymph nodes; SPL, spleen.

markers, such as CD80, CD86, and HLA-DR, on iPSC-derived cDC1s (*SI Appendix*, Fig. S6*I*). These results demonstrate that cDC1 differentiation was successfully induced by this method. Upon DOX stimulation, iPSC-derived cDC1s showed significantly higher *GPR31* expression (Fig. 3*D*).

To investigate whether dendrite protrusion of PA-stimulated human intestinal cDC1s was induced by GPR31 activation, changes in cell morphology under the PA stimulation were evaluated using GPR31-expressing iPSC-derived cDC1s. Morphological changes in GPR31-expressing iPSC-derived cDC1s were observed, including a significant increase in the percentage of cells with dendrite extension, during PA stimulation (Fig. 3*E*). Dendrite extension in iPSC-derived cDC1s without DOX stimulation also tended to increase during PA stimulation, possibly in relation to endogenous

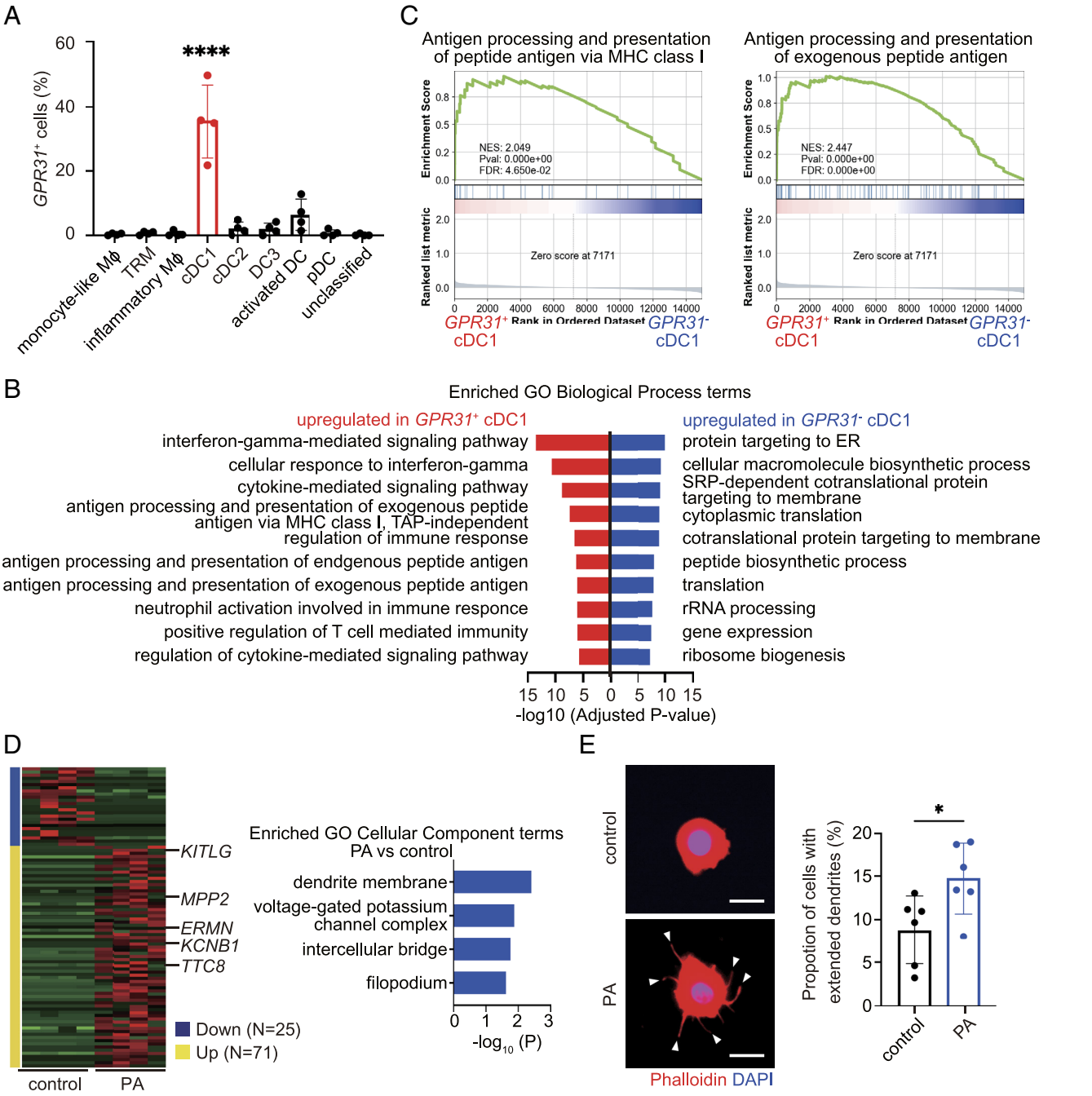

Fig. 2. GPR31 activation upon stimulation with the bacterial metabolite pyruvate. (*A*) Percentages of *GPR31*$^+$ cells among cDC1s and other MNP subsets, determined via scRNA-seq analysis of MNPs from human ileal lamina propria (mean ± SD of four independent experiments). ****$P < 0.0001$. Statistical analysis via one-way ANOVA followed by Tukey's multiple comparison test. (*B*) Bar graph of the top 10 enriched GO Biological Process 2021 terms that were significantly up-regulated in *GPR31*$^+$ cDC1s compared with *GPR31*$^-$ cDC1s or *GPR31*$^-$ cDC1s compared with *GPR31*$^+$ cDC1s, determined via scRNA-seq analysis of MNPs from human ileal lamina propria. (*C*) GSEA of gene sets enriched in *GPR31*$^+$ cDC1s compared with *GPR31*$^-$ cDC1s. NES, normalized enrichment score; FDR, false discovery rate. (*D*) *Left*: Heatmap of differentially expressed genes in human intestinal cDC1s upon stimulation with 100 μM PA (n = 4 in each group), determined via bulk RNA-seq analysis. *Right*: Enriched GO Cellular Component terms that were significantly up-regulated in the PA stimulation group. (*E*) *Left*: Representative morphology of human ileal cDC1s upon stimulation with 100 μM PA for 4 h. Arrowheads indicate extended dendrites. Red, phalloidin; blue, DAPI. (Scale bar, 10 μm.) *Right*: Percentage of cDC1s with extended dendrites (mean ± SD of six independent experiments). Percentages of cells with dendrite length > 5 μm were quantified. *$P < 0.05$. Statistical analysis by two-tailed unpaired Student's *t* test.

GPR31 expression in iPSC-derived cDC1s (*SI Appendix*, Fig. S6*F*). On the other hand, general activation of DCs by LPS stimulation did not affect dendrite extension (*SI Appendix*, Fig. S7*A*) (36). Furthermore, PA-induced dendrite protrusion was canceled under treatment with NF449, a Gsα-subunit-selective G-protein antagonist (*SI Appendix*, Fig. S7*B*) (37). These results indicate that PA stimulation promotes GPR31-dependent dendrite protrusion of human intestinal cDC1s.

cDC1s Extended Dendrites into Interepithelial Space via the PA–GPR31 Axis. Next, to explore the physiological significance of cDC1 dendrite extension, we examined the localization of cDC1s in the human small intestine. Immunohistochemical analysis showed that some XCR1$^+$ cDC1s were localized immediately under intestinal epithelia (Fig. 4*A*) and extended dendrites between epithelial layers (Fig. 4*B*). These data indicate that cDC1s may recognize some gut luminal substances through epithelial gaps. Based on the

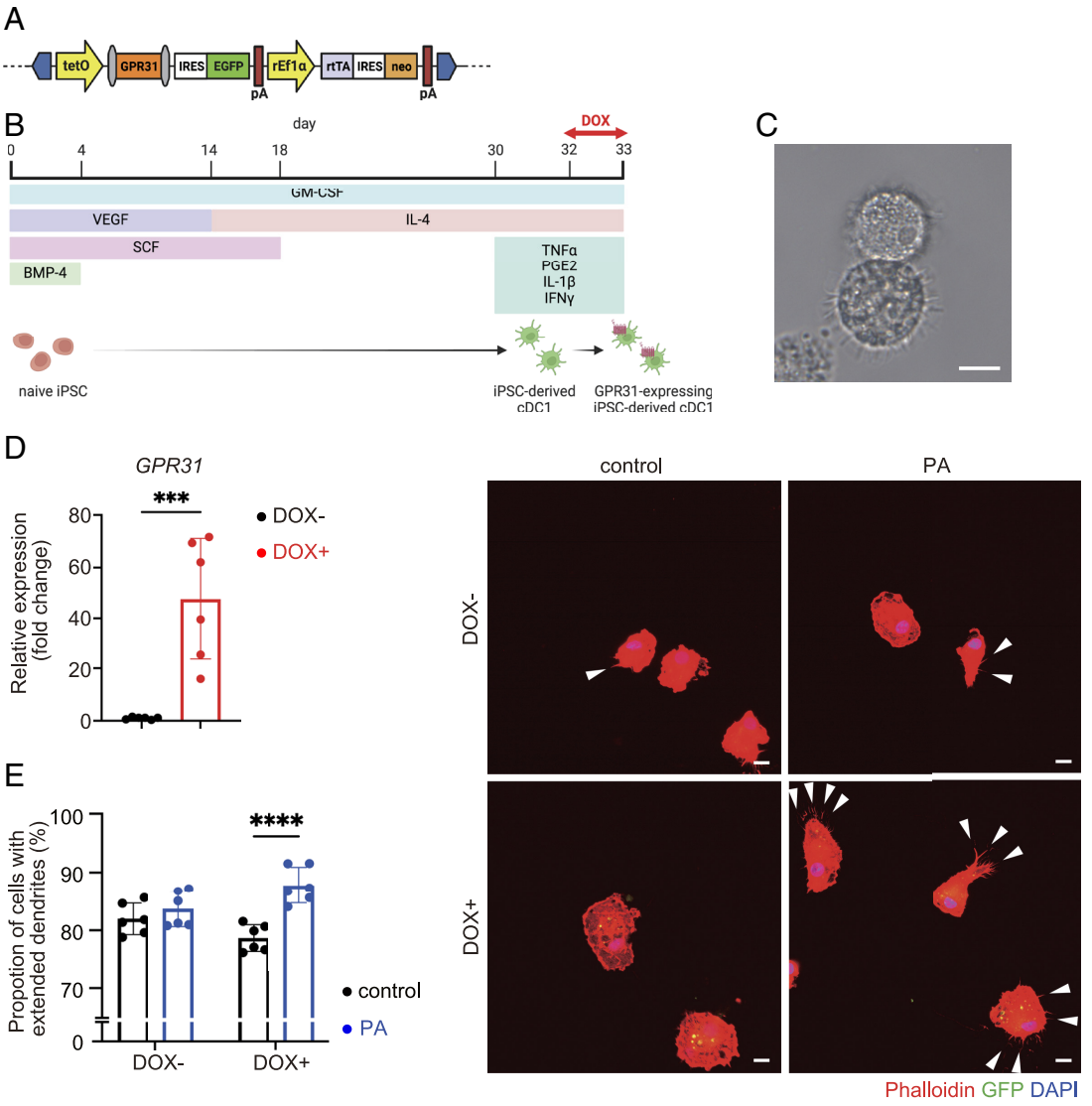

Fig. 3. Generation of human iPSC-derived cDC1s with drug-inducible *GPR31*. (*A*) Schematic representation of the construction of a drug-inducible *GPR31* expression vector based on the *piggyBac* transposon (PB-TAG-ERN) used in this study. The tetracycline resistance operon (tetO), *GPR31* gene, internal ribosomal entry site (IRES), enhanced green fluorescence protein (EGFP), polyadenylation signal (pA), rat elongation factor 1α promoter sequences (rEf1α), reverse tetracycline transactivator gene (rtTA), and neomycin resistance gene (neo) are shown. (*B*) Schematic representation of the protocol for iPSC differentiation into cDC1s. (*C*) Morphology of iPSC-derived cDC1s observed via bright-field microscopy. (Scale bar, 10 μm.) (*D*) Relative expression of *GPR31* in GPR31-expressing iPSC-derived cDC1s (DOX^+) and control cDC1s (DOX^-) (mean ± SD of six independent experiments). ***$P < 0.001$. Statistical analysis by two-tailed unpaired Student's *t* test. (*E*) *Left*: Percentage of cDC1s with extended dendrites (mean ± SD of six independent experiments). Percentages of cells with dendrite length >5 μm were quantified. ****$P < 0.0001$. Statistical analysis via two-way ANOVA followed by Sidak's multiple comparison test. *Right*: Representative morphology of iPSC-derived cDC1s upon stimulation with 100 μM PA for 4 h. Arrowheads indicate extended dendrites. Red, phalloidin; green, GFP; blue, DAPI. (Scale bar, 10 μm.)

immunohistochemical results, we established a three-dimensional (3D) culture model using cell culture inserts to determine whether cDC1s extend dendrites toward higher concentrations of PA. When PA was added to the chamber opposite from human ileal primary cDC1s, we found that cDC1s extended their dendrites toward PA (Fig. 4*C*). To evaluate whether GPR31 is involved in this process, we utilized a similar model involving GPR31-expressing iPSC-derived cDC1s. The percentage of cells with dendrite protrusion toward PA was significantly increased after PA stimulation in GPR31-expressing iPSC-derived cDC1s, suggesting that cDC1s extend dendrites toward PA via GPR31 (Fig. 4*D*).

To reproduce physical and functional barriers between the gut lumen and cDC1s, we established a coculture model of cDC1s and intestinal epithelium (38). Intestinal organoids derived from the human small intestine were cultured as monolayers on cell culture inserts opposite from primary cDC1s until they reached full confluence (*SI Appendix*, Fig. S8). PA stimulation of the epithelial chamber led to TED formation of intestinal cDC1s (Fig. 4*E*). Additionally, when a similar model was established using iPSC-derived cDC1s, GPR31-expressing iPSC-derived cDC1s showed dendrite protrusion into the interepithelial space during PA stimulation (Fig. 4*F*). In contrast, iPSC-derived cDC1s without GPR31 induction demonstrated minimal TED formation regardless of PA stimulation. These results suggest that intestinal cDC1s extend dendrites through interepithelial gaps via PA-mediated GPR31 activation.

cDC1s Internalized Antigens via the PA–GPR31 Axis. In the next experiment, we investigated whether antigen recognition and uptake by $GPR31^+$ cDC1s were efficiently achieved via the PA–GPR31 axis. GPR31-expressing iPSC-derived cDC1s were cultured on the membranes of cell culture inserts; medium with ovalbumin (OVA) was placed in the chamber opposite from cDC1s. Antigen uptake

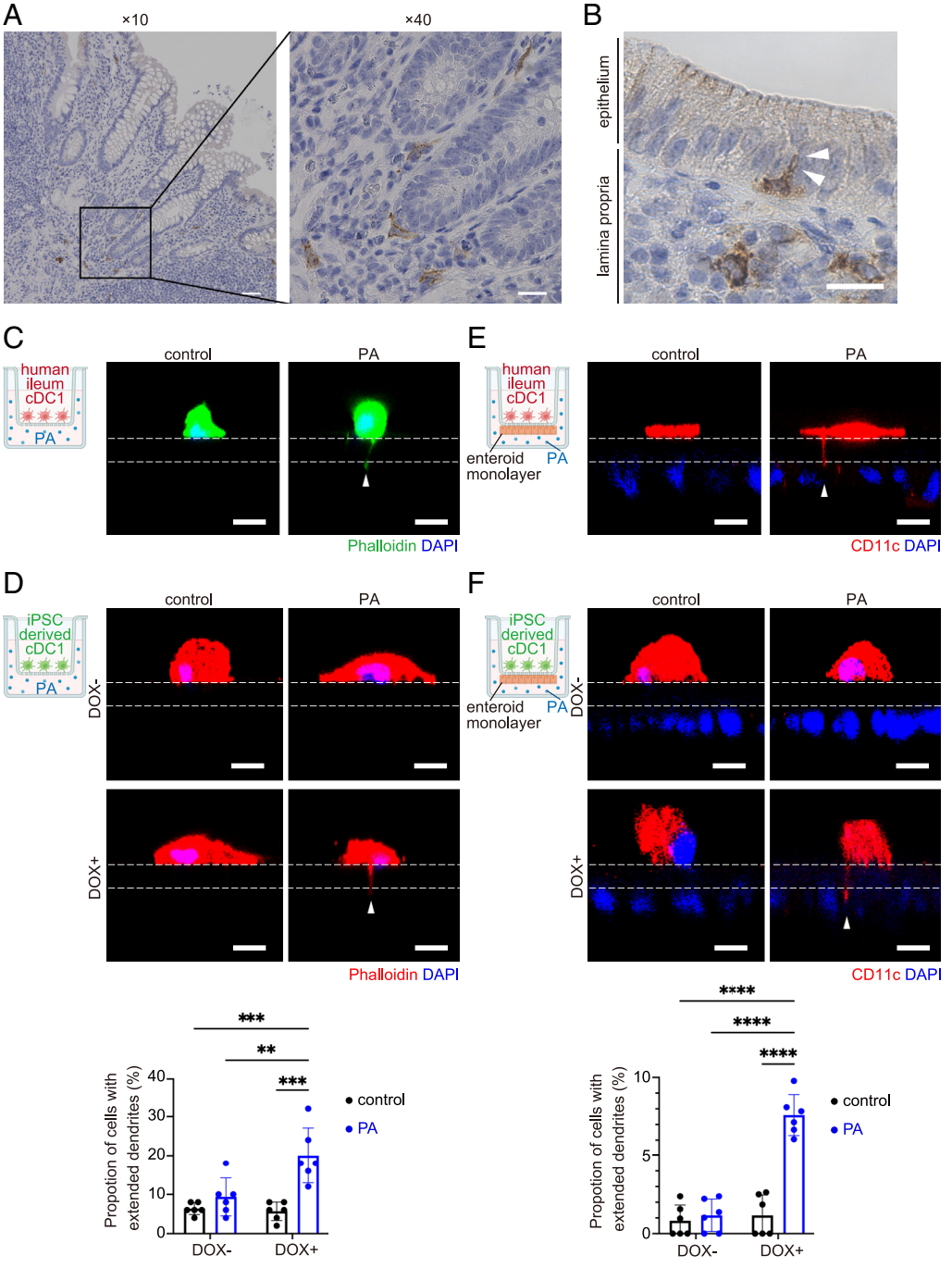

Fig. 4. Human intestinal cDC1s extended dendrites into interepithelial space via the pyruvate–GPR31 axis. (*A* and *B*) Immunohistochemical staining of XCR1 expression in the human ileum. (*A*) *Left*: Scale bar, 50 μm. *Right*: Scale bar, 20 μm. (*B*) cDC1s extended dendrites into interepithelial space (arrowheads). (Scale bar, 20 μm.) (*C* and *D*) 3D culture model. cDC1s were seeded onto 1.0-μm pore insert filters; 1 mM PA was added to the lower chamber and cells were cultured for 1 h. cDC1s extended dendrites across the 1.0-μm pore insert filter to reach the lower chamber during PA stimulation (arrowheads). Dashed lines indicate the position of 1.0-μm pore insert filter. (Scale bar, 10 μm.) (*C*) 3D culture model using human ileal cDC1s. Green, phalloidin; blue, DAPI. (*D*) *Top*: 3D culture model using iPSC-derived cDC1s. Red, phalloidin; blue, DAPI. *Bottom*: Percentage of cells with extended dendrites in 3D culture model using iPSC-derived cDC1s (mean ± SD of six independent experiments). Percentages of cells with dendrites extending through the membrane to the lower chamber were quantified. $^{**}P < 0.01$; $^{***}P < 0.001$. Statistical analysis via two-way ANOVA followed by Tukey's multiple comparison test. (*E* and *F*) Coculture model of cDC1s (upper chamber) and enteroid monolayer (lower chamber). After 1 mM PA was added to the lower chamber, cells were cultured for 1 h. cDC1s extended dendrites across the 1.0-μm pore insert filter to reach the enteroid monolayer during PA stimulation (arrowheads). Red, CD11c; blue, DAPI. (Scale bar, 10 μm.) (*E*) Coculture model using human ileal cDC1s. (*F*) *Top*: Coculture model using iPSC-derived cDC1s. *Bottom*: Percentage of cells with extended dendrites in 3D culture model using iPSC-derived cDC1s (mean ± SD of six independent experiments). Percentages of cells with dendrites extending into the epithelial layer were quantified. $^{****}P < 0.0001$. Statistical analysis via two-way ANOVA followed by Tukey's multiple comparison test.

analysis revealed that the percentage of OVA^+ cells displaying antigen uptake was significantly increased among GPR31-expressing iPSC-derived cDC1s during PA stimulation (Fig. 5*A*). Increased antigen uptake was not observed by LPS stimulation and was canceled by the Gsα antagonist NF449, suggesting that antigen uptake in cDC1s was promoted in a GPR31-dependent manner, but not by general activation of DC (*SI Appendix*, Fig. S7*C*). Despite the presence of an epithelial barrier, antigen uptake on the opposite side was observed in GPR31-expressing iPSC-derived cDC1s during PA stimulation (Fig. 5*B*). In contrast, antigen uptake was not observed in iPSC-derived cDC1s without GPR31 induction, regardless of PA stimulation. Furthermore, GPR31-expressing iPSC-derived cDC1s demonstrated uptake of killed *Escherichia coli* (*E. coli*) on the epithelial side (Fig. 5*C*). These results indicated that the recognition and uptake of intraluminal antigens (e.g., bacteria or dietary components) by human intestinal cDC1s were enhanced by increased TED protrusion into the lumen via the PA–GPR31 axis.

cDC1s are known to cross-prime $CD8^+$ T cells (39), and coimmunostaining of $XCR1^+$ cDC1s and $CD8^+$ T cells in healthy mucosa of the human small intestine revealed that some cDC1s in close proximity to epithelial cells were in contact with $CD8^+$ T cells, suggesting that cDC1 recognition of intraluminal antigens promotes activation to $CD8^+$ T cells (*SI Appendix*, Fig. S9). Thus, whether cDC1s enhances the activation of gut-derived $CD8^+$ T cells via the PA-GPR31 axis was investigated. cDC1s were precultured with killed *E. coli* in the presence or absence of PA using a 3D culture model to enable cDC1s to take up the antigen. Subsequently, these cDC1s were washed and cocultured with

human intestinal CD8$^+$ T cells isolated from the same individuals. cDC1s precultured with killed *E. coli* in the presence of PA activated CD8$^+$ T cells more strongly than cDC1s precultured in the absence of PA (Fig. 5*D*). Taken together, these findings indicate that human cDC1s present immediately under intestinal epithelia extend dendrites into the lumen and uptake luminal antigens, thereby modulating the activation of CD8$^+$ T cells.

Discussion

GPR31, identified in 1997 (40), was initially classified as a class A orphan GPCR (24). Then, 12(S)-HETE was identified as a ligand for GPR31 (27). Subsequently, the 12(S)-HETE–GPR31 axis demonstrated roles in inflammation (41), tumor progression (42, 43), pancreatic organogenesis (44), platelet activation (45), and fibrosis (46). Recent studies have indicated that GPR31 can also detect protons (47); GPR31 expression in mouse intestinal epithelium enables recognition of intestinal acidosis, a process involved in the onset of inflammation (48). We previously showed that oral administration of PA or LA (both gut bacterial metabolites) induces dendrite protrusion via GPR31 expressed on CX3CR1$^+$ myeloid cells in mouse small intestine, thereby enhancing resistance to *Salmonella* infection (17). Furthermore, oral administration of PA can induce oral tolerance via GPR31 expressed on CX3CR1$^+$ myeloid cells in mouse small intestine (49). All of these findings support functional regulation of murine CX3CR1$^+$ myeloid cells by the LA/PA–GPR31 axis; however, GPR31-expressing cells have not been identified in human intestinal immune cells, hindering application of these findings in clinical practice. Our analysis of human MNPs revealed that PA stimulates GPR31 expressed on human cDC1s, as well dendrite protrusion of cDC1s into the intestinal lumen.

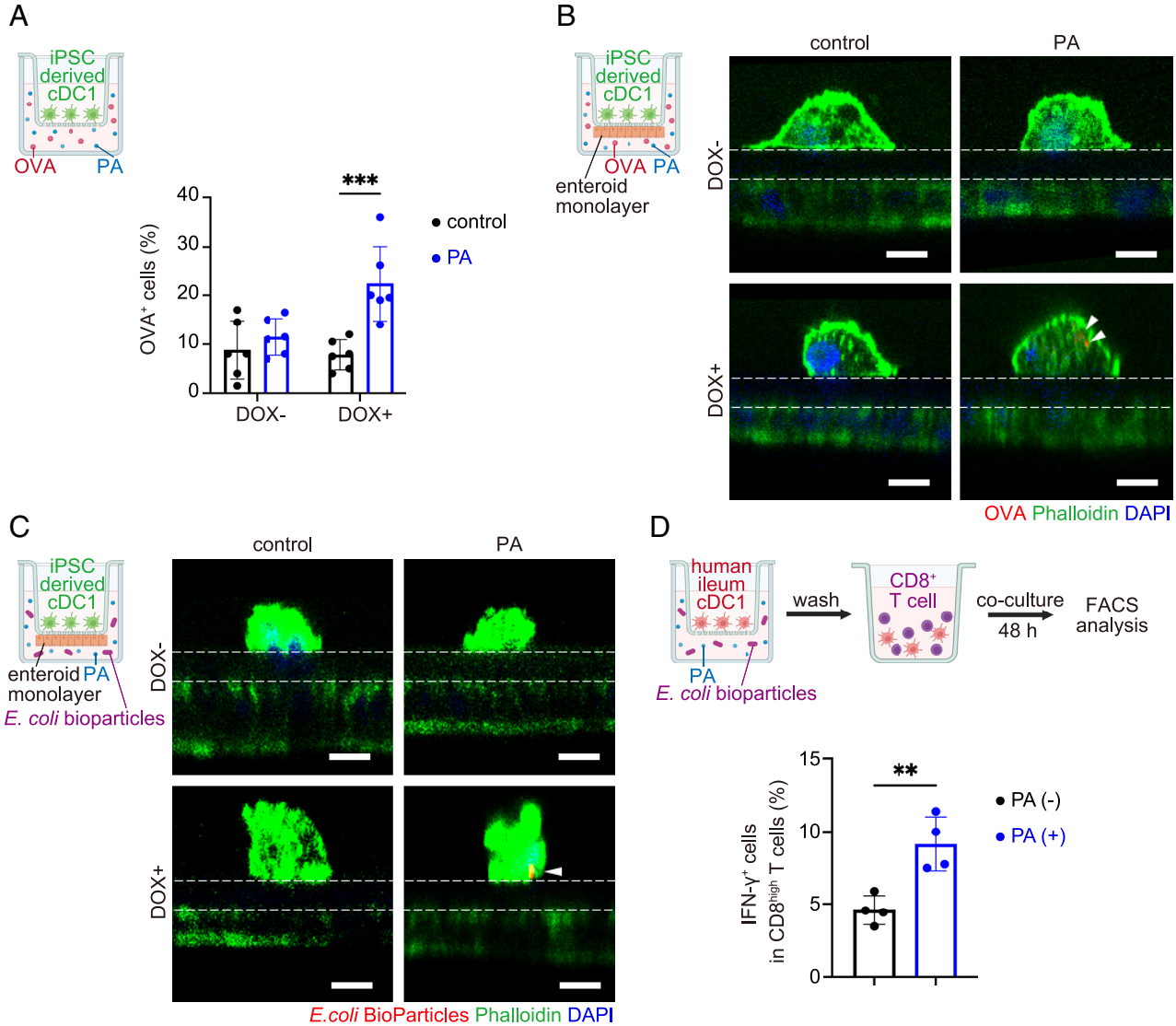

Fig. 5. Human intestinal cDC1s internalized antigens via the pyruvate–GPR31 axis. (*A*) Percentage of OVA$^+$ iPSC-derived cDC1s (mean ± SD of six independent experiments). OVA (10 μg/mL) was added to the chamber opposite from induced cDC1s and cells were cultured for 1 h. ***$P < 0.001$. Statistical analysis via two-way ANOVA followed by Sidak's multiple comparison test. (*B*) Coculture model of iPSC-derived cDC1s (upper chamber) and enteroid monolayer (lower chamber). PA (1 mM) and OVA (10 μg/mL) were added to the lower chamber and cells were cultured for 1 h. Arrowheads indicate OVA uptaken by GPR31-expressing iPSC-derived cDC1s. Red, OVA; green, phalloidin; blue, DAPI. (Scale bar, 10 μm.) (*C*) Coculture model of iPSC-derived cDC1s (upper chamber) and enteroid monolayer (lower chamber). PA (1 mM) and Alexa Fluor 594-conjugated *E. coli* (K-12 strain) BioParticles (20 μg/mL) were added to the lower chamber and cells were cultured for 1 h. Arrowheads indicate *E. coli* phagocytosed by GPR31-expressing induced cDC1s. Red, *E. coli* BioParticles; green, phalloidin; blue, DAPI. (Scale bar, 10 μm.) (*D*) Coculture model of human intestinal cDC1s and human intestinal CD8$^+$ T cells. PA (1 mM) and *E. coli* (K-12 strain) BioParticles (20 μg/mL) were added to the lower chamber and cells were precultured for 1 h. cDC1s were washed and cocultured with human intestinal CD8$^+$ T cells for 48 h. Percentages of IFN-γ$^+$ cells in CD8^{high} T cells were obtained by FACS analysis (mean ± SD of four independent experiments). **$P < 0.01$. Statistical analysis by two-tailed unpaired Student's *t* test.

DC dendrite formation requires conformational changes in the actin cytoskeleton (50). Coverslip experiments involving monocyte-derived human DCs showed that dendrite formation requires the interaction of β1-integrin (CD29) on the DC surface with fibronectin in the extracellular matrix, combined with the cooperative activities of Rho GTPases (RhoA, Rac1, and Cdc42) (51, 52). Additionally, particularly in the gut, a barrier of epithelial cells (closely bound via tight junctions) on the luminal surface restricts mucosal entry of luminal contents. Intriguingly, tissue-specific factors (i.e., metabolites from gut commensal microbes) promote dendrite protrusion within the specialized intestinal tract environment.

Antigen-presenting cell (APC)-mediated rapid sensing of luminal antigens is necessary for protection against pathogens and maintenance of intestinal homeostasis; representative mechanisms include TED formation by APCs (53), goblet cell-associated antigen passage (54), and transcytosis by microfold cells (M cells) (55, 56). TED formation allows APCs to directly access intraluminal antigens; for example, DCs in mouse small intestinal lamina propria express tight junction proteins that allow dendrite protrusion into the intestinal lumen for bacterial monitoring purposes without disruption of the epithelial barrier (53). Other studies have shown that $CD11c^+$ DCs and $CD103^+$ DCs in mouse small intestine form TEDs via MyD88-dependent Toll-like receptor signaling (57, 58). Furthermore, $CX3CR1^+$ DCs in mouse intestine exhibit CX3CR1-dependent dendrite protrusion into the intestinal lumen and sampling of luminal antigens; this phenomenon is diminished by depletion of the intestinal microbiota (16, 59). Thus far, most analyses of TED formation have been conducted in mice. Considering that the characteristics of immune cells in the gut are not necessarily conserved between humans and mice (60, 61), studies involving human immune cells are needed for clinical application of these experimental findings.

In mice, *Gpr31* expression is regulated by the CX3CL1-CX3CR1 axis (17) and *Gpr31* is expressed in $CX3CR1^+$ myeloid cells. However, according to our MNP dataset and previous reports in humans, *CX3CR1* expression levels do not align with that of *GPR31* and not highly expressed on cDC1s (62, 63). To date, the regulatory factors of *GPR31* expression in humans have not yet been elucidated, and it is likely that different mechanisms other than the CX3CL1-CX3CR1 axis underlie the transcriptional regulation of *GPR31* in the human intestine. While $CX3CR1^+$ myeloid cells are developmentally, transcriptionally and phenotypically distinct from the cDC1, both are involved in immune surveillance and antigen presentation; $CX3CR1^+$ macrophages are involved in the transfer of antigens to migratory DCs for presentation to T cells (64), while cDC1s are specialized in cross-presentation of antigens to $CD8^+$ T cells and activation of Th1 cells (39, 65). It is not clear why this apparently distinct cell type in mice and humans promotes dendrite protrusion through the same mechanism, but there may be an advantage in favoring the PA-GPR31 axis over others in certain cellular functions. One hypothesis is that GPR31 is associated with cellular localization, such as adjacency to the intestinal epithelium, and hence GPR31 signaling is favored for TED formation promoted by gut luminal cues in various cell types. The fact that the effect of the PA-GPR31 axis on TED formation was conserved across species regardless of myeloid cell types suggests that GPR31 may play a role in bridging the gap between species in essential biological processes established in previous studies. Additionally, our present study implies that GPR31-expressing cDC1s sample intraluminal antigens and activate $CD8^+$ T cells. Given that antigen processing by $CX3CR1^+$ myeloid cells in the lamina propria in mice has been shown to activate $CD8^+$ T cells and vice versa (66, 67), it is thus interesting to speculate that GPR31 is involved in these processes. A previous report has shown that mouse immune cell classification does not always align with that of humans, but some transcriptional bases are conserved (63). Correspondence of immune cell subsets across species based on these transcriptional footprints will pave the way for translating animal studies into the human immune cell analyses. Overall, activation of GPR31 in human intestinal cDC1s enables active recognition of intestinal bacteria and antigens to enhance intestinal barrier function, suggesting that the PA–GPR31 axis has value as a drug discovery target. Further studies are needed to determine whether the PA–GPR31 axis in humans is also involved in the induction of oral tolerance, as previously reported in mice (49).

Probiotics, such as *Lactobacillus*, and symbiotics such as *Bifidobacterium lactis* and fructooligosaccharides are widely used for host health benefits; these agents have been reported to produce (or facilitate the production of) PA or LA (68, 69). Furthermore, engineered probiotics, which efficiently produce metabolites such as LA, have recently been developed and are expected to have therapeutic applications (70). Since human GPR31 was shown to respond to LA as well as PA (17), our results suggest that the administration of PA- and LA-producing probiotics can promote GPR31-mediated antigen recognition by cDC1s, thereby increasing protection against infection. Mucosal vaccines are useful formulations because, in addition to the systemic response, they provide an enhanced response at the mucosal surface by inducing antigen-specific secretory IgA antibody production. Furthermore, they do not require an invasive administration method, and they are currently licensed for protection from several pathogens, including *Vibrio cholerae*, *Salmonella* Typhimurium, poliovirus, and rotavirus (71, 72). Considering that efficient antigen recognition by APCs is important for mucosal vaccine effectiveness (72), the PA–GPR31 axis is expected to be a useful target.

In summary, this study revealed that the PA–GPR31 axis plays an important role in luminal antigen recognition by human small intestinal cDC1s. The enhancement of luminal antigen recognition via the PA–GPR31 axis is expected to have clinical applications, such as protection from infection and improvements in mucosal vaccine efficacy.

Materials and Methods

Isolation of Intestinal Lamina Propria Cells. Ileal intestinal mucosa was surgically obtained from patients with colorectal cancer or Crohn's disease (CD). Unaffected ileal mucosa from colorectal cancer patients were used for analyses unless otherwise noted. For bulk RNA-seq analyses and PA stimulation experiments involving isolated human cDC1s, ileal mucosa from CD patients were used to obtain a sufficient number of cells for analysis. Briefly, intestinal epithelial cells were dissociated by shaking in 5 mM ethylenediaminetetraacetic acid (EDTA) in Hanks' Balanced Salt Solution (HBSS), followed by removal of the muscle layer. The mucosal layer was cut into pieces and digested in RPMI 1640 containing 4% fetal bovine serum, 0.8 mg/mL collagenase D (Roche, Basel, Switzerland), 0.8 mg/mL dispase (Thermo Fisher Scientific, Waltham, MA), and 70 U/mL DNase I (Sigma-Aldrich, St. Louis, MO) for 60 min at 37 °C in a shaking water bath. The digested tissues were resuspended in 7 mL of 20% Percoll and overlaid on 2 mL of 40% Percoll in a 15-mL tube. Percoll gradient separation was performed via centrifugation at 500 g for 30 min at 4 °C. Lamina propria cells at the interface of the Percoll gradient were collected and washed with phosphate-buffered saline (PBS) containing 2% fetal bovine serum.

Isolation of GALT-Free Lamina Propria Cells. GALT-free lamina propria cells were isolated by a previously described method (73). Briefly, mesenteric fat, serosal layer, and external muscles were trimmed off from surgically obtained human ileum samples. Samples were shaken in 5 mM EDTA in HBSS. Isolated lymphoid follicles were identified under the transilluminated microscope as round follicular structures obscuring the intestinal crypts and were excised using

a scalpel. Subsequent methods were the same as those described in the "Isolation of intestinal lamina propria cells" section.

Flow Cytometry. The following antibodies were purchased from BioLegend (San Diego, CA): fluorescein isothiocyanate (FITC)-conjugated anti-human CD3 (HIT3a), FITC-conjugated anti-human CD14 (M5E2), FITC-conjugated anti-human CD19 (HIB19), FITC-conjugated anti-human CD20 (2H7), FITC-conjugated anti-human CD56 (HCD56), FITC-conjugated anti-human CD123 (6H6), FITC-conjugated anti-human CD326 (EpCAM) (9C4), PE-conjugated anti-human XCR1 (S15046E), PE-conjugated anti-human CD14 (HCD14), PE-conjugated anti-human CD86 (10.1), PE-conjugated anti-human CD141 (M80), PE-conjugated anti-human CD172a (SIRPα) (15-414), PE-conjugated anti-human TCRγ/δ (B1), PE-conjugated Mouse IgG1, κ Isotype Ctrl (MOPC-21), PE-conjugated Mouse IgG2a, κ Isotype Ctrl (MOPC-173), PE/cyanine7-conjugated anti-human HLA-DR (L243), PE/cyanine7-conjugated anti-human CD8 (SK1), APC-conjugated anti-human CD8b (S21011A), APC/Fire 750-conjugated anti-human CD11c (S-HCL-3), APC/cyanine7-conjugated anti-human CD3 (UCHT1), Pacific Blue-conjugated anti-human CD45 (2D1), Pacific Blue-conjugated anti-human CD123 (6H6), and BV421-conjugated anti-human XCR1 (S15046E). PE-conjugated anti-human CD80 (L307.4), PE-conjugated anti-human HLA-DR (L243), PE-conjugated Mouse IgG2b κ Isotype Control (27-35), APC-conjugated anti-human CD11c (B-ly6), and APC-conjugated anti-human CD45 (HI30) were purchased from BD Biosciences (Franklin Lakes, NJ). Dead cells were stained with 7-AAD Viability Staining Solution (BioLegend). Flow cytometry analysis was performed with a FACSCanto II flow cytometer (BD Biosciences) using FlowJo software (Tree Star, Ashland, OR). $7AAD^-CD3^-CD19^-CD20^-CD56^-EpCAM^-CD45^+HLA\text{-}DR^+$ human intestinal MNPs, $7AAD^-CD3^-CD14^-CD19^-CD20^-CD56^-CD123^-EpCAM^-CD45^+HLA\text{-}DR^+CD11c^+XCR1^+$ human intestinal cDC1s, $7AAD^-CD3^-CD14^-CD19^-CD20^-CD56^-CD123^-EpCAM^-CD45^+HLA\text{-}DR^+CD11c^+SIRP\alpha^+$ human intestinal cDC2s, $7AAD^-CD3^-CD19^-CD20^-CD56^-EpCAM^-CD45^+HLA\text{-}DR^+CD14^+$ human intestinal Mϕs, $7AAD^-CD3^-CD11c^-CD14^-CD19^-CD20^-CD56^-EpCAM^-CD45^+HLA\text{-}DR^+CD123^+$ human intestinal pDCs, $7AAD^-CD3^+CD8^+CD8b^-TCR\gamma/\delta^-$ human intestinal $CD8^+$ T cells and $7AAD^-CD11c^+XCR1^+$ iPSC-derived cDC1s were isolated using a FACSAria flow cytometer (BD Biosciences).

scRNA-seq Library Preparation (10× Chromium). Normal ileal intestinal mucosa was obtained from macroscopically intact areas in patients with colorectal cancer. Lamina propria cells were freshly prepared from surgically resected samples and incubated with Human TruStain FcX (BioLegend) for 10 min at 4 °C. Subsequently, cells were stained with cell surface markers for 30 min at 4 °C and then subjected to dead cell staining. Cells from SI3 samples were labeled with TotalSeq-C0251 anti-human Hashtag 1 antibody (BioLegend) for ileal cells and TotalSeq-C0252 anti-human Hashtag 2 antibody (BioLegend) for colon cells; these labels were applied simultaneously during surface marker staining. Cells from SI4 samples were labeled with TotalSeq-C0253 anti-human Hashtag 3 antibody (BioLegend) for ileal cells and TotalSeq-C0252 anti-human Hashtag 2 antibody (BioLegend) for colon cells; these labels were applied simultaneously during surface marker staining. $7AAD^-CD3^-CD19^-CD20^-CD56^-EpCAM^-CD45^+HLA\text{-}DR^+$ human intestinal MNPs were sorted on a BD FACSAria. Cells were resuspended in PBS with 1% bovine serum albumin at a density of 1,000 cells/μL. Single-cell droplets were generated by 10× Genomics Chromium Controller (10× Genomics, Pleasanton, CA), and complementary DNAs (cDNAs) with unique molecular identifiers (UMIs) were generated at the single-cell level. Single-cell libraries were prepared in accordance with the protocol described in the Chromium Single Cell 5′ Reagent Kits v2 User Guide (10× Genomics). The libraries were sequenced on a NovaSeq 6000 (Illumina, San Diego, CA).

scRNA-seq Analysis (10× Chromium). Sequencing data were preprocessed and aligned with Cell Ranger v.6.0.0 (10× Genomics). For SI3 and SI4 data, cells labeled with hashtags for ileal cells were extracted using R 4.1.2, Seurat 4.1.0, Scanpy 1.9.1, and python 3.9.12 and then used for analysis. Quantified expression data were preprocessed and visualized using Scanpy 1.9.1 and python 3.9.12. Cells were filtered out if they had mitochondrial genes >20%, total counts > 40,000, or detected genes > 6,000. After data normalization and the detection of highly variable genes, dimensionality reduction was performed via principal component analysis. Sample batch effects were removed by the Scanorama algorithm. Cells were clustered using the Leiden algorithm and cell clusters were visualized with the UMAP algorithm. These Leiden-based cell clusters were manually annotated using well-known cell type–specific genes. Gene set enrichment analysis (GSEA) was performed using the prerank tool in GSEApy.

Targeted scRNA-seq Library Preparation (BD Rhapsody). Normal ileal intestinal mucosa was obtained from macroscopically intact areas in the patient with colorectal cancer. Lamina propria cells were freshly prepared from surgically resected samples and incubated with Human TruStain FcX (BioLegend) for 5 min at 4 °C. Subsequently, cells were stained with cell surface markers for 20 min at 4 °C and then subjected to dead cell staining. $7AAD^-CD3^-CD19^-CD20\text{-}CD56^-EpCAM^-CD45^+HLA\text{-}DR^+$ human intestinal MNPs were sorted on a BD FACSAria. Single-cell suspensions were loaded onto BD Rhapsody (BD Biosciences) and bead libraries were loaded onto corresponding cartridges. Cells were lysed to hybridize mRNAs onto barcoded capture oligos on the beads. The beads were collected in a single tube for the subsequent steps of cDNA synthesis, exonuclease I digestion, and multiplex PCR-based library construction. The BD Rhapsody Human Immune Response Panel and a custom primer set (*SI Appendix*, Table S2) were used for library generation. Libraries were sequenced on the NovaSeq 6000 platform.

scRNA-seq Analysis (BD Rhapsody). The BD Rhapsody Analysis Pipeline was used to process sequencing data (fastq files). Data were converted to h5ad files using R 4.1.2 and Seurat 4.1.0. Quantified expression data were preprocessed and visualized using Scanpy 1.9.1 and python 3.9.12. Cells with <3 detected genes were filtered out. After data normalization and the detection of highly variable genes, dimensionality reduction was performed via principal component analysis. Cells were clustered using the Leiden algorithm and cell clusters were visualized with the UMAP algorithm. These Leiden-based cell clusters were manually annotated using well-known cell type–specific genes. Clusters consisting mainly of $CD3E^+$ T cells, $CD79A^+$ B cells, or $CPA3^+$ mast cells were excluded prior to analysis.

scRNA-seq (Public Data). The scRNA-seq dataset of human immune cells in systemic organs was collected from the Cross-tissue Immune Cell Atlas (https://www.tissueimmunecellatlas.org) (25). Cells were annotated according to dataset designation. During analysis of *GPR31* expression in organ-specific cDC1 subsets, organs with <20 cDC1s were excluded. During analysis of *GPR31* expression in organ-specific immune cell populations, organs without *GPR31*-expressing cells were excluded. Quantified expression data were preprocessed and visualized using Scanpy 1.9.1 and python 3.9.12.

Bulk RNA-seq. Human intestinal cDC1s isolated from the ileum of CD patients were sorted on a BD FACSAria and then stimulated with the indicated reagents at 37 °C for 1 h. 500 to 1,000 cells for human intestinal cDC1 were used for analysis in each stimulation group. In the analysis of RNA-seq–based gene expression values for *GPR31* in each MNP subset of the human ileum, macrophages, cDC1s, cDC2s, and pDCs were isolated from unaffected ileal intestinal mucosa of colorectal cancer patients. Cells were lysed with TRIzol Reagent (Thermo Fisher Scientific). Full-length cDNA was generated using a SMART-Seq HT Kit (Takara Bio, Kusatsu, Japan). In accordance with the SMARTer kit instructions, Illumina libraries were prepared using a NexteraXT DNA Library Preparation Kit (Illumina). Sequencing was performed on a NovaSeq 6000 platform (Illumina) in 101-base single-end mode. Generated reads were mapped to the human (hg19) reference genome using TopHat v2.1.1 in combination with Bowtie2 v2.2.8 and SAMtools v0.1.18. Read count data were analyzed using iDEP.96 (http://bioinformatics.sdstate.edu/idep96/) (74, 75); hierarchical clustering and principal component analysis were performed, followed by selection of differentially expressed genes (false discovery rate < 0.1) by DESeq2 (76). GO Cellular Component terms enriched for these differentially expressed genes were identified using Metascape v3.5.20230501 (https://metascape.org/) (77).

Real-Time Reverse Transcription (RT)-PCR. Total RNA was isolated using the GenElute Mammalian Total RNA Miniprep Kit (Sigma-Aldrich); the RNA was reverse transcribed with ReverTra Ace qPCR RT Master Mix with gDNA Remover (Toyobo, Osaka, Japan). Real-time RT-PCR was performed on a Step One Plus™ Real-Time PCR System (Applied Biosystems, Waltham, MA) using GoTaq qPCR Master Mix (Promega, Madison, WI). All values were normalized to the expression of the *GAPDH* gene (encoding glyceraldehyde-3-phosphate dehydrogenase), and fold differences relative to *GAPDH* expression were

recorded. The amplification conditions were 50 °C (2 min), 95 °C (10 min), and 40 cycles of 95 °C (15 s) and 64 °C (60 s). The following primer sets were used: *GAPDH*, 5′-gtctcctctgacttcaacagcg-3′ and 5′-accaccctgttgctgtagccaa-3′; *GPR31*, 5′-cgtacgctgtctacctgctc-3′ and 5′-ttgaccttaagccgagggtg-3′, *XCR1*, 5′- gctgtgattattccgaact-3′ and 5′- catagagcaccgggtta-3′.

Assessment of Dendrite Protrusion. cDC1s were incubated in a fibronectin (Corning, Corning, NY)-coated 96-well glass-bottom plate (AGC Techno Glass, Shizuoka, Japan) at 37 °C overnight and then stimulated with the indicated reagents for 4 h. Next, the cells were fixed with 4% paraformaldehyde (PFA) for 20 min at 37 °C. They were washed three times in PBS and permeabilized with 0.1% Triton-X/PBS. After one wash with PBS, cells were stained with 1 μM tetramethylrhodamine (TRITC)-phalloidin (Sigma-Aldrich) in PBS at room temperature for 45 min in the dark. Nuclei were counterstained with DAPI (Fluoro-KEEPER Antifade Reagent, Nacalai Tesque, Kyoto, Japan). Cell images were automatically acquired (300 pictures per well at 40× magnification) using an IN Cell analyzer 6000 (GE Healthcare, Chicago, IL). Percentages of TRITC and DAPI double-positive cells with dendrite length >5 μm were quantified using IN Cell Investigator Developer Toolbox 1.10.0 (GE Healthcare) and IN Carta image analysis software (GE Healthcare). In experiments with LPS stimulation, cells were stimulated by 10 ng/mL LPS from *E. coli* O55:B5 (Sigma-Aldrich) for 24 h. In experiments with Gsα subunit-selective G protein antagonists, 10 μM NF449 (MedChemExpress, Monmouth Junction, NJ, USA) was preadministered 30 min prior to PA stimulation.

siRNA. Human intestinal cDC1s in the ileum of colorectal cancer patients or CD patients were sorted on a BD FACSAria and then cultured with 1 μM of smart pool Accell siRNA targeting human *GPR31* [Accell Human GPR31 (2853) siRNA; E-005564-00-0005; Dharmacon, Lafayette, CO] or 1 μM of Accell nontargeting control (Accell Non-targeting Pool; D-001910-10-05, Dharmacon) at 37 °C with 5% CO2 for 72 h.

Human iPS Cell Line and Cell Culture. The human iPS cell line (1231A3) used in this study was provided by the RIKEN Bioresource Research Center (Tsukuba, Japan). The original material, established by Kyoto University, was derived from ePBMCs that had been purchased from Cellular Technology Limited (https://immunospot.com/). Six-well plates were coated with laminin-511 E8 fragment (Nippi, Tokyo, Japan). iPSCs were seeded in the plates at a density of 1.2×10^4 cells/well and then maintained in StemFit AK02N medium (ReproCELL, Yokohama, Japan) containing 10 μM Y-27632 (Nacalai Tesque) for 1 d. Y-27632-free culture medium was used beginning on day 2. The 1231A3 line was passaged weekly using TrypLE Express (Thermo Fisher Scientific) for dissociation and 10 μM Y-27632 to facilitate adhesion after passage. Routine cell line testing was performed to ensure cells remained *Mycoplasma*-free.

Preparation of a *piggyBac* Vector for *GPR31* Expression and Introduction into iPSCs. *GPR31*-iPSCs were generated using a previously described method (78). Briefly, human *GPR31* cDNA was cloned and inserted into the pENTR vector (Thermo Fisher Scientific). *GPR31* cDNA was transferred into PB-TAG-ERN (plasmid #80474; Addgene, Watertown, MA) with Gateway cloning technology to generate *piggyBac* vectors. Semiconfluent iPSCs maintained under feeder-free conditions were dissociated into single cells by TrypLE Express (Thermo Fisher Scientific). Next, 1.0×10^6 cells were electroporated with 1 μg of PB-TAG-ERN plus 1 μg of transposase expression vector (pCMV-hyPBase) using the following poring pulse settings: 125 v, 5 ms pulse, 50 ms gap, 2 pulse, and 10% decay (+ pulse orientation); and the following transfer pulse settings: 20 v, 50 ms pulse, 50 ms gap, 5 pulse, and 40% decay (± pulse orientation). Electroporated cells were plated in six-well plates in StemFit AK02N medium (ReproCELL) containing 10 μM Y-27632 (Nacalai Tesque). Two days after transfection, the medium was replaced with fresh medium containing 100 μg/mL G418 (Nacalai Tesque) and cultured for 8 to 10 d until iPSC colonies appeared. iPSC colonies were picked from plates and expanded in the presence of G418. After clone selection, iPSCs carrying the DOX-inducible GPR31 construct (*GPR31*-iPSCs) were established.

Differentiation into cDC1s. iPSC-derived cDC1s were differentiated from *GPR31*-iPSCs using a previously described method (33, 34). Briefly, the differentiation medium consisted of XVIVO-15 (Lonza, Slough, UK) supplemented with nonessential amino acids (FUJIFILM Wako, Osaka, Japan), 2 mM L-glutamine (Thermo Fisher Scientific), 1 mM sodium pyruvate (Nacalai Tesque), 50 μM 2-mercaptoethanol (Thermo Fisher Scientific), 50 ng/mL granulocyte-macrophage colony-stimulating factor (GM-CSF) (PeproTech, London, UK), 20 ng/mL stem cell factor (R&D Systems, Abingdon, UK), 50 ng/mL vascular endothelial growth factor (VEGF) (PeproTech), and 50 ng/mL bone morphogenetic protein-4 (R&D Systems). Bone morphogenetic protein-4 was removed from day 5 onward, followed by VEGF (day 14) and stem cell factor (day 19). On days 13 to 17 of culture, the medium was supplemented with 25 ng/mL interleukin (IL)-4 (PeproTech). The concentration of IL-4 in the medium was increased to 100 ng/mL (days 20 to 24). cDC1s were harvested on day 26 and then plated in six-well plates (MS-80060; Sumitomo Bakelite, Tokyo, Japan) containing complete XVIVO-15 medium with 50 ng/mL GM-CSF and 100 ng/mL IL-4. After 4 d, DCs were matured for the final 48 h of culture using a cytokine cocktail comprising 50 ng/mL tumor necrosis factor-α (R&D Systems), 1 μg/mL prostaglandin E2 (Sigma-Aldrich), 10 ng/mL IL-1β (R&D Systems), and 20 ng/mL interferon-γ (R&D Systems). iPSC-derived cDC1s was cultured in the presence of 1 μL/mL DOX for at least 24 h to express *GPR31*. Images of iPSC-derived cDC1 morphology were acquired using an All-in-One Fluorescence Microscope (BZ-X810; Keyence) and processed using a BZ-X800 Analyzer (Keyence).

Immunohistochemistry. Normal ileal intestinal mucosa was obtained from macroscopically intact areas in patients with colorectal cancer. The tissue was fixed with 4% PFA and then embedded in paraffin. Ileal samples were sectioned at a thickness of 4 μm. For 3,3-diaminobenzidine (DAB) staining, immunohistochemistry was performed with an anti-human XCR1 antibody (Clone D2F8T; Cell Signaling Technology, Danvers, MA) (1:800 dilution), using a DAKO EnVision™ FLEX Mini Kit, High pH (Agilent Technologies, Santa Clara, CA), in accordance with the manufacturer's instructions. In double staining analysis, slides were stained with PermaRed/AP-AutoPlus (Diagnostic BioSystems, Pleasanton, CA) using the ImmPRESS®-AP Horse Anti-Mouse IgG Polymer Detection Kit (Vector Laboratories, Newark, CA), along with an anti-human CD8 antibody (Clone C8/144B; Agilent Technologies) (1:100 dilution). Images were acquired using an All-in-One Fluorescence Microscope (BZ-X810; Keyence) and processed using a BZ-X800 Analyzer (Keyence).

3D Culture Model. cDC1s were cultured in fibronectin (Corning)-coated cell culture insert filters (Corning; 24-well inserts, 1.0-μm pore polyethylene terephthalate membrane) at 37 °C overnight. Medium containing the indicated reagents was added to the chamber opposite from cells, and the cells were incubated for 1 h. Cells were subsequently fixed with 4% PFA for 30 min at 37 °C. Cells were washed three times in PBS and permeabilized with 0.1% Triton-X/PBS. After one wash with PBS, cells were stained with 1 μM FITC-phalloidin (Sigma-Aldrich) or 1 μM TRITC-phalloidin (Sigma-Aldrich) in PBS at room temperature for 45 min in the dark. Nuclei were counterstained with DAPI (Nacalai Tesque). Images were acquired using a confocal laser scanning microscope (LSM710, Zeiss, Oberkochen, Germany) under a 63× oil objective. To quantify cells with extended dendrites, the percentages of TRITC and DAPI double-positive cells with dendrites extending into the lower chamber were quantified by collecting z-stack images of all cells on the filter. Images were processed using ZEN 2011 SP7 FP3 (Black Edition) imaging software (Zeiss).

Establishment of Human Enteroids. Human enteroids were established from a surgically resected sample of normal human ileum. After removal of the muscle layer, the intestinal layers were washed in PBS and minced into small pieces, washed again in PBS, and incubated at room temperature until the minced tissues precipitated. Gentle Cell Dissociation Reagent (STEMCELL Technologies, Vancouver, Canada) was added to the precipitates; the mixtures were shaken at 40 rpm on ice for 30 min and then centrifuged at 290 g for 5 min. Dulbecco's modified Eagle medium (DMEM)/Ham's F12 (Nacalai Tesque) supplemented with 1% fetal bovine serum was added to the precipitates and mixed by thorough pipetting; the mixtures were filtered with a 100-μm cell strainer and centrifuged at 200 g for 5 min. Cells were dissolved in DMEM/Ham's F12 mixed with Matrigel (Corning) at a ratio of 1:1 and seeded in 24-well plates. After the Matrigel had solidified, IntestiCult Organoid Growth Medium (STEMCELL Technologies) supplemented with 100 U/mL penicillin, 100 μg/mL streptomycin, and 10 μM Y-27632 (Nacalai Tesque) was added; cultures were incubated at 37 °C. The medium was changed every 2 to 3 d, and enteroids were passaged every 7 d.

Establishment of Human Enteroid Monolayers. Human enteroid monolayers were established using a previously described method with slight modification (79). Briefly, the bottom surfaces of cell culture insert filters (Corning; 24-well

inserts, 1.0-μm pore polyethylene terephthalate membrane) were coated with 2% Matrigel (Corning) solution and incubated at 37 °C for 1 h. Seven-day-old enteroid cultures were harvested from Matrigel domes using Gentle Cell Dissociation Reagent (STEMCELL Technologies) and incubated at 37 °C for 5 min in 0.05% trypsin–EDTA to dissociate organoids into single cells. The cells were resuspended in IntestiCult Organoid Growth Medium supplemented with 100 U/mL penicillin, 100 μg/mL streptomycin, and 10 μM Y-27632 (Nacalai Tesque). The cell suspension was then seeded onto the bottom surface of precoated cell culture insert filters and incubated at 37 °C for 1 h. After this incubation, the inserts were returned to their original position in a 24-well receiver plate; medium was added to the insert and the well. The medium was changed every 2 to 3 d, and enteroid cultures reached confluency in 5 to 7 d.

cDC1–Enteroid Coculture. cDC1s were seeded in laminin-511 E8 fragment (Nippi)-coated cell culture insert filters containing an enteroid monolayer. Medium containing the indicated reagents was added to the monolayer side of the chamber and cells were incubated for 1 h. Next, the cells were fixed with 4% PFA for 30 min at 37 °C. Cells were washed three times in PBS and permeabilized with 0.1% Triton-X/PBS and then subjected to blocking with 1% bovine serum albumin in PBS for 30 min at room temperature and staining with anti-CD11c antibody (Abcam, Cambridge, UK) for 18 h at 4 °C. Cells were then washed three times in PBS and incubated with Alexa 647–conjugated anti-mouse IgG antibody (Invitrogen, Carlsbad, CA) for 1 h at room temperature. After one wash with PBS, nuclei were counterstained with DAPI (Nacalai Tesque). Images were acquired using a confocal laser scanning microscope (LSM710, Zeiss) under a 63× oil objective and processed using ZEN 2011 SP7 FP3 (Black Edition) imaging software (Zeiss).

Antigen Uptake Analysis. cDC1s were seeded in laminin-511 E8 fragment (Nippi)-coated cell culture insert filters containing an enteroid monolayer. Medium containing the indicated reagents and 10 μg/mL Alexa Fluor 647–conjugated ovalbumin (Thermo Fisher Scientific) or 20 μg/mL Alexa Fluor 594–conjugated *E. coli* (K-12 strain) BioParticles (Thermo Fisher Scientific) was added to the monolayer side of the chamber and cells were incubated for 1 h. Next, the cells were fixed with 4% PFA for 30 min at 37 °C. Cells were washed three times in PBS and permeabilized with 0.1% Triton-X/PBS. After one wash with PBS, cells were stained with 1 μM FITC-phalloidin (Sigma-Aldrich) in PBS at room temperature for 45 min in the dark. Nuclei were counterstained with DAPI (Nacalai Tesque). Images were acquired using a confocal laser scanning microscope (LSM710, Zeiss) under a 63× oil objective. To quantify cells taken up antigens, the percentages of Alexa Fluor 647 or Alexa Fluor 594 and DAPI double-positive cells were measured by collecting images of all cells on the filter. Images were processed using ZEN 2011 SP7 FP3 (Black Edition) imaging software (Zeiss).

cDC1–CD8$^+$ T Cell Coculture. Human intestinal cDC1s from the ileum of colorectal cancer patients or CD patients were sorted on a BD FACSAria and then seeded in laminin-511 E8 fragment (Nippi)-coated cell culture insert filters. Medium containing the indicated reagents and 20 μg/mL killed *E. coli* was added to the opposite side of cells. Alexa Fluor 594–conjugated *E. coli* (K-12 strain) BioParticles (Thermo Fisher Scientific) was used as killed *E. coli*. Cells were precultured for 4 h. Next, cDC1s were washed and cocultured with human intestinal CD8$^+$ T cells isolated from the same individuals for 48 h. The ratios of CD8$^+$ T cells to cDC1s were 2:1. Intracellular expression of IFN-γ in intestinal CD8$^+$ T cells was analyzed by using a Cytofix/Cytoperm Plus Kit with GolgiStop (BD Biosciences), in accordance with the manufacturer's instructions. In brief, the cells were incubated in the presence of GolgiStop at 37 °C for 4 h. After surface staining, cells were permeabilized with Cytofix/Cytoperm solution (BD Biosciences) and stained with anti–IFN-γ antibodies (B27; BioLegend). Data acquisition was performed on a BD FACSCanto II flow cytometer (BD Biosciences). The percentage of IFN-γ$^+$ cells in CD8^{high} T cells was analyzed with FlowJo software (Tree Star).

Ethical Approval and Informed Consent. All human gut samples used in this study were collected from patients who underwent surgery for colon cancer or Crohn's disease at the Department of Gastroenterological Surgery, Graduate School of Medicine, Osaka University, and the Department of Gastroenterological Surgery, Division of Inflammatory Bowel Disease Surgery, Hyogo Medical University. This study was approved by the Ethical Committees of Osaka University School of Medicine (549) and Hyogo Medical University (0407); written informed consent for sample use was obtained from all participants.

Statistical Analysis. Statistical analyses were performed with GraphPad Prism 9.4.0 (GraphPad Software) unless otherwise stated. Statistical parameters (including the value of n with a description of what it represents, along with the mean and SD) are reported in the figures and figure legends. Unless otherwise stated, statistical significance was determined by two-tailed unpaired Student's *t* test or two-tailed paired Student's *t* test for two groups or by one-way ANOVA followed by Sidak's or Tukey's multiple comparison test for multiple groups. *P*-values < 0.05 were considered statistically significant.

Data, Materials, and Software Availability. The data underlying Figs. 1 and 2 and *SI Appendix*, Figs. S1, S2, and S5 (scRNA-seq [10× Chromium]) are openly available in at the NCBI's Gene Expression Omnibus under the accession number GSE240900 (80). The data underlying *SI Appendix*, Fig. S3 (scRNA-seq [BD Rhapsody]) are openly available in at the NCBI's Gene Expression Omnibus under the accession number GSE242091 (81). The data underlying *SI Appendix*, Fig. S3 (bulk RNA-seq of each MNP subset) are openly available in at the NCBI's Gene Expression Omnibus under the accession number GSE272657 (82). The data underlying Fig. 2 and *SI Appendix*, Fig. S5 (bulk RNA-seq of intestinal cDC1) are openly available in at the NCBI's Gene Expression Omnibus under the accession number GSE240895 (83). Previously published data were used for this work (25).

ACKNOWLEDGMENTS. This work was supported by Grants-in-Aid for Scientific Research (JP21H050430 to K.T. and JP21K07895 to M.M.), the Japan Agency for Medical Research and Development (JP21gm1010004 to K.T.), JST SPRING (JPMJSP2138 to E.O.-I.), and the Multicolor FACS Technology Development Support Program (J178501002 to M.M.). We thank all patients and medical staff at Osaka University and Hyogo Medical University who contributed to this study. We are also grateful to Yuri Terao (Center for Medical Research and Education, Graduate School of Medicine, Osaka University) and Yui Magota (Immunology Frontier Research Center, Osaka University) for technical assistance and to Chisa Hidaka (Immunology Frontier Research Center, Osaka University) and Miki Yamaguchi (Hyogo Medical University) for administrative assistance. We thank all members of the Takeda lab for their useful comments that improved this study. Schematic representations were created with biorender.com. We thank Ryan Chastain-Gross, Ph.D., from Edanz (https://jp.edanz.com/ac) for editing a draft of this manuscript.

Author affiliations: [a]Department of Microbiology and Immunology, Graduate School of Medicine, Osaka University, Osaka 565-0871, Japan; [b]World Premier International Research Center Initiative (WPI) Immunology Frontier Research Center, Osaka University, Osaka 565-0871, Japan; [c]Department of Respiratory Medicine and Clinical Immunology, Graduate School of Medicine, Osaka University, Osaka 565-0871, Japan; [d]Department of Gastroenterological Surgery, Graduate School of Medicine, Osaka University, Osaka 565-0871, Japan; [e]Department of Gastroenterological Surgery, Division of Inflammatory Bowel Disease Surgery, Hyogo Medical University, Hyogo 663-8501, Japan; [f]Department of Surgical Pathology, Hyogo Medical University, Hyogo 663-8501, Japan; [g]Department of Pathology, Osaka University Graduate School of Medicine, Osaka University, Osaka 565-0871, Japan; [h]Department of Pediatrics, Graduate School of Medicine, Osaka University, Osaka 565-0871, Japan; [i]Department of Infection Metagenomics, Genome Information Research Center, Research Institute for Microbial Diseases, Osaka University, Osaka 565-0871, Japan; [j]Integrated Frontier Research for Medical Science Division, Institute for Open and Transdisciplinary Research Initiatives, Osaka University, Osaka 565-0871, Japan; [k]Division of Microbiology and Immunology, Center for Infectious Disease Education and Research, Osaka University, Osaka 565-0871, Japan; [l]Center for Advanced Modalities and Drug Delivery System, Osaka University, Osaka 565-0871, Japan; [m]Laboratory of Microbiology and Immunology, School of Pharmaceutical Sciences, University of Shizuoka, Shizuoka 422-8526, Japan; and [n]Department of Immunopathology, World Premier International Research Center Initiative (WPI) Immunology Frontier Research Center, Osaka University, Osaka 565-0871, Japan

1. R. Sender, S. Fuchs, R. Milo, Revised estimates for the number of human and bacteria cells in the body. *PLoS Biol.* **14**, e1002533 (2016).
2. K. Oliphant, E. Allen-Vercoe, Macronutrient metabolism by the human gut microbiome: Major fermentation by-products and their impact on host health. *Microbiome* **7**, 91 (2019).
3. K. A. Krautkramer, J. Fan, F. Backhed, Gut microbial metabolites as multi-kingdom intermediates. *Nat. Rev. Microbiol.* **19**, 77–94 (2021).
4. A. Agus, K. Clement, H. Sokol, Gut microbiota-derived metabolites as central regulators in metabolic disorders. *Gut* **70**, 1174–1182 (2021).
5. A. S. Husted, M. Trauelsen, O. Rudenko, S. A. Hjorth, T. W. Schwartz, GPCR-mediated signaling of metabolites. *Cell Metab.* **25**, 777–796 (2017).
6. J. K. Tan, C. McKenzie, E. Marino, L. Macia, C. R. Mackay, Metabolite-sensing G protein-coupled receptors–facilitators of diet-related immune regulation. *Annu. Rev. Immunol.* **35**, 371–402 (2017).

7. L. J. Cohen *et al.*, Functional metagenomic discovery of bacterial effectors in the human microbiome and isolation of commendamide, a GPCR G2A/132 agonist. *Proc. Natl. Acad. Sci. U.S.A.* **112**, E4825–E4834 (2015).
8. L. J. Cohen *et al.*, Commensal bacteria make GPCR ligands that mimic human signalling molecules. *Nature* **549**, 48–53 (2017).
9. H. Chen *et al.*, A forward chemical genetic screen reveals gut microbiota metabolites that modulate host physiology. *Cell* **177**, 1217–1231.e18 (2019).
10. H. Chen *et al.*, Highly multiplexed bioactivity screening reveals human and microbiota metabolome-GPCRome interactions. *Cell* **186**, 3095–3110.e19 (2023).
11. A. Chow, B. D. Brown, M. Merad, Studying the mononuclear phagocyte system in the molecular age. *Nat. Rev. Immunol.* **11**, 788–798 (2011).
12. R. Elmentaite *et al.*, Cells of the human intestinal tract mapped across space and time. *Nature* **597**, 250–255 (2021).
13. L. Zhang *et al.*, Single-cell analyses inform mechanisms of myeloid-targeted therapies in colon cancer. *Cell* **181**, 442–459.e29 (2020).
14. D. Domanska *et al.*, Single-cell transcriptomic analysis of human colonic macrophages reveals niche-specific subsets. *J. Exp. Med.* **219**, e20211846 (2022).
15. A. Garrido-Trigo *et al.*, Macrophage and neutrophil heterogeneity at single-cell spatial resolution in human inflammatory bowel disease. *Nat. Commun.* **14**, 4506 (2023).
16. J. H. Niess *et al.*, CX3CR1-mediated dendritic cell access to the intestinal lumen and bacterial clearance. *Science* **307**, 254–258 (2005).
17. N. Morita *et al.*, GPR31-dependent dendrite protrusion of intestinal CX3CR1(+) cells by bacterial metabolites. *Nature* **566**, 110–114 (2019).
18. A. Bujko *et al.*, Transcriptional and functional profiling defines human small intestinal macrophage subsets. *J. Exp. Med.* **215**, 441–458 (2018).
19. K. Asano *et al.*, Intestinal CD169(+) macrophages initiate mucosal inflammation by secreting CCL8 that recruits inflammatory monocytes. *Nat. Commun.* **6**, 7802 (2015).
20. S. De Schepper *et al.*, Self-maintaining gut macrophages are essential for intestinal homeostasis. *Cell* **175**, 400–415.e13 (2018).
21. J. C. Martin *et al.*, Single-cell analysis of Crohn's disease lesions identifies a pathogenic cellular module associated with resistance to anti-TNF therapy. *Cell* **178**, 1493–1508.e20 (2019).
22. A. C. Villani *et al.*, Single-cell RNA-seq reveals new types of human blood dendritic cells, monocytes, and progenitors. *Science* **356**, eaah4573 (2017).
23. P. Bourdely *et al.*, Transcriptional and functional analysis of CD1c(+) human dendritic cells identifies a CD163(+) subset priming CD8(+)CD103(+) T Cells. *Immunity* **53**, 335–352.e8 (2020).
24. S. P. Alexander *et al.*, THE CONCISE GUIDE TO PHARMACOLOGY 2021/22: G protein-coupled receptors. *Br. J. Pharmacol.* **178** (suppl. 1), S27–S156 (2021).
25. C. Dominguez Conde *et al.*, Cross-tissue immune cell analysis reveals tissue-specific features in humans. *Science* **376**, eabl5197 (2022).
26. J. Cosin-Roger, D. Ortiz-Masia, M. D. Barrachina, S. Calatayud, Metabolite sensing GPCRs: Promising therapeutic targets for cancer treatment? *Cells* **9**, 2345 (2020).
27. Y. Guo *et al.*, Identification of the orphan G protein-coupled receptor GPR31 as a receptor for 12-(S)-hydroxyeicosatetraenoic acid. *J. Biol. Chem.* **286**, 33832–33840 (2011).
28. H. Kress *et al.*, Filopodia act as phagocytic tentacles and pull with discrete steps and a load-dependent velocity. *Proc. Natl. Acad. Sci. U.S.A.* **104**, 11633–11638 (2007).
29. P. Hellman, H. Eriksson, Early activation markers of human peripheral dendritic cells. *Hum. Immunol.* **68**, 324–333 (2007).
30. M. Cabeza-Cabrerizo, A. Cardoso, C. M. Minutti, M. Pereira da Costa, C. Reis e Sousa, Dendritic cells revisited. *Annu. Rev. Immunol.* **39**, 131–166 (2021).
31. A. T. Prechtel, A. Steinkasserer, CD83: An update on functions and prospects of the maturation marker of dendritic cells. *Arch. Dermatol. Res.* **299**, 59–69 (2007).
32. K. Woltjen *et al.*, piggyBac transposition reprograms fibroblasts to induced pluripotent stem cells. *Nature* **458**, 766–770 (2009).
33. K. M. Silk *et al.*, Cross-presentation of tumour antigens by human induced pluripotent stem cell-derived CD141(+)XCR1+ dendritic cells. *Gene Ther.* **19**, 1035–1040 (2012).
34. P. Sachamitr, A. J. Leishman, T. J. Davies, P. J. Fairchild, Directed differentiation of human induced pluripotent stem cells into dendritic cells displaying tolerogenic properties and resembling the CD141(+) subset. *Front. Immunol.* **8**, 1935 (2017).
35. D. A. Anderson III, C. A. Dutertre, F. Ginhoux, K. M. Murphy, Genetic models of human and mouse dendritic cell development and function. *Nat. Rev. Immunol.* **21**, 101–115 (2021).
36. T. De Smedt *et al.*, Regulation of dendritic cell numbers and maturation by lipopolysaccharide in vivo. *J. Exp. Med.* **184**, 1413–1424 (1996).
37. M. Hohenegger *et al.*, Gsalpha-selective G protein antagonists. *Proc. Natl. Acad. Sci. U.S.A.* **95**, 346–351 (1998).
38. G. Noel *et al.*, A primary human macrophage-enteroid co-culture model to investigate mucosal gut physiology and host-pathogen interactions. *Sci. Rep.* **7**, 45270 (2017).
39. J. M. den Haan, S. M. Lehar, M. J. Bevan, CD8(+) but not CD8(-) dendritic cells cross-prime cytotoxic T cells in vivo. *J. Exp. Med.* **192**, 1685–1696 (2000).
40. A. Zingoni *et al.*, Isolation and chromosomal localization of GPR31, a human gene encoding a putative G protein-coupled receptor. *Genomics* **42**, 519–523 (1997).
41. X. J. Zhang *et al.*, An ALOX12-12-HETE-GPR31 signaling axis is a key mediator of hepatic ischemia-reperfusion injury. *Nat. Med.* **24**, 73–83 (2018).
42. K. V. Honn *et al.*, 12-HETER1/GPR31, a high-affinity 12(S)-hydroxyeicosatetraenoic acid receptor, is significantly up-regulated in prostate cancer and plays a critical role in prostate cancer progression. *FASEB J.* **30**, 2360–2369 (2016).
43. F. Yang *et al.*, Ischemia reperfusion injury promotes recurrence of hepatocellular carcinoma in fatty liver via ALOX12-12HETE-GPR31 signaling axis. *J. Exp. Clin. Cancer Res.* **38**, 489 (2019).
44. M. Hernandez-Perez *et al.*, A 12-lipoxygenase-Gpr31 signaling axis is required for pancreatic organogenesis in the zebrafish. *FASEB J.* **34**, 14850–14862 (2020).
45. L. Van Doren *et al.*, Lipid receptor GPR31 (G-protein-coupled receptor 31) regulates platelet reactivity and thrombosis without affecting hemostasis. *Arterioscler. Thromb. Vasc. Biol.* **41**, e33–e45 (2021).
46. M. Rubino *et al.*, Inhibition of eicosanoid degradation mitigates fibrosis of the heart. *Circ. Res.* **132**, 10–29 (2023).
47. M. Mashiko, A. Kurosawa, Y. Tani, T. Tsuji, S. Takeda, GPR31 and GPR151 are activated under acidic conditions. *J. Biochem.* **166**, 317–322 (2019).
48. I. M. Cartwright *et al.*, Mucosal acidosis elicits a unique molecular signature in epithelia and intestinal tissue mediated by GPR31–induced CREB phosphorylation. *Proc. Natl. Acad. Sci. U.S.A.* **118**, e2023871118 (2021).
49. Q. Liu *et al.*, Pyruvate enhances oral tolerance via GPR31. *Int. Immunol.* **34**, 343–352 (2022).
50. S. Burns, A. J. Thrasher, M. P. Blundell, L. Machesky, G. E. Jones, Configuration of human dendritic cell cytoskeleton by Rho GTPases, the WAS protein, and differentiation. *Blood* **98**, 1142–1149 (2001).
51. C. A. Swetman *et al.*, beta1-Integrins determine the dendritic morphology which enhances DC-SIGN-mediated particle capture by dendritic cells. *Int. Immunol.* **18**, 1295–1303 (2006).
52. C. A. Swetman *et al.*, Extension, retraction and contraction in the formation of a dendritic cell dendrite: Distinct roles for Rho GTPases. *Eur. J. Immunol.* **32**, 2074–2083 (2002).
53. M. Rescigno *et al.*, Dendritic cells express tight junction proteins and penetrate gut epithelial monolayers to sample bacteria. *Nat. Immunol.* **2**, 361–367 (2001).
54. J. R. McDole *et al.*, Goblet cells deliver luminal antigen to CD103+ dendritic cells in the small intestine. *Nature* **483**, 345–349 (2012).
55. M. R. Neutra, A. Frey, J. P. Kraehenbuhl, Epithelial M cells: Gateways for mucosal infection and immunization. *Cell* **86**, 345–348 (1996).
56. D. H. Kulkarni, R. D. Newberry, Intestinal macromolecular transport supporting adaptive immunity. *Cell Mol. Gastroenterol. Hepatol.* **7**, 729–737 (2019).
57. M. Chieppa, M. Rescigno, A. Y. Huang, R. N. Germain, Dynamic imaging of dendritic cell extension into the small bowel lumen in response to epithelial cell TLR engagement. *J. Exp. Med.* **203**, 2841–2852 (2006).
58. J. Farache *et al.*, Luminal bacteria recruit CD103+ dendritic cells into the intestinal epithelium to sample bacterial antigens for presentation. *Immunity* **38**, 581–595 (2013).
59. J. H. Niess, G. Adler, Enteric flora expands gut lamina propria CX3CR1+ dendritic cells supporting inflammatory immune responses under normal and inflammatory conditions *J. Immunol.* **184**, 2026–2037 (2010).
60. E. R. Mann *et al.*, Intestinal dendritic cells: Their role in intestinal inflammation, manipulation by the gut microbiota and differences between mice and men. *Immunol. Lett.* **150**, 30–40 (2013).
61. D. L. Gibbons, J. Spencer, Mouse and human intestinal immunity: Same ballpark, different players; different rules, same score. *Mucosal. Immunol.* **4**, 148–157 (2011).
62. S. Hiddingh *et al.*, Transcriptome network analysis implicates CX3CR1-positive type 3 dendritic cells in non-infectious uveitis. *Elife* **12**, e74913 (2023).
63. C. C. Brown *et al.*, Transcriptional basis of mouse and human dendritic cell heterogeneity. *Cell* **179**, 846–863.e24 (2019).
64. E. Mazzini, L. Massimiliano, G. Penna, M. Rescigno, Oral tolerance can be established via gap junction transfer of fed antigens from CX3CR1(+) macrophages to CD103(+) dendritic cells. *Immunity* **40**, 248–261 (2014).
65. S. L. Jongbloed *et al.*, Human CD141+ (BDCA-3)+ dendritic cells (DCs) represent a unique myeloid DC subset that cross-presents necrotic cell antigens. *J. Exp. Med.* **207**, 1247–1260 (2010).
66. S. Y. Chang *et al.*, Circulatory antigen processing by mucosal dendritic cells controls CD8(+) T cell activation. *Immunity* **38**, 153–165 (2013).
67. Y. I. Kim *et al.*, CX(3)CR1(+) macrophages and CD8(+) T cells control intestinal IgA production. *J. Immunol.* **201**, 1287–1294 (2018).
68. A. Ljungh, T. Wadstrom, Lactic acid bacteria as probiotics. *Curr. Issues Intest. Microbiol.* **7**, 73–89 (2006).
69. L. Crovesy, T. El-Bacha, E. L. Rosado, Modulation of the gut microbiota by probiotics and symbiotics is associated with changes in serum metabolite profile related to a decrease in inflammation and overall benefits to metabolic health: A double-blind randomized controlled clinical trial in women with obesity. *Food Funct.* **12**, 2161–2170 (2021).
70. L. M. Sanmarco *et al.*, Lactate limits CNS autoimmunity by stabilizing HIF-1alpha in dendritic cells. *Nature* **620**, 881–889 (2023).
71. N. Lycke, Recent progress in mucosal vaccine development: Potential and limitations. *Nat. Rev. Immunol.* **12**, 592–605 (2012).
72. E. C. Lavelle, R. W. Ward, Mucosal vaccines–Fortifying the frontiers. *Nat. Rev. Immunol.* **22**, 236–250 (2022).
73. P. B. Jorgensen *et al.*, Identification, isolation and analysis of human gut-associated lymphoid tissues. *Nat. Protoc.* **16**, 2051–2067 (2021).
74. S. X. Ge, E. W. Son, R. Yao, iDEP: An integrated web application for differential expression and pathway analysis of RNA-Seq data. *BMC Bioinformatics* **19**, 534 (2018).
75. X. Ge, iDEP web application for RNA-seq data analysis. *Methods Mol. Biol.* **2284**, 417–443 (2021).
76. M. I. Love, W. Huber, S. Anders, Moderated estimation of fold change and dispersion for RNA-seq data with DESeq2. *Genome Biol.* **15**, 550 (2014).
77. Y. Zhou *et al.*, Metascape provides a biologist-oriented resource for the analysis of systems-level datasets. *Nat. Commun.* **10**, 1523 (2019).
78. S. I. Kim *et al.*, Inducible transgene expression in human iPS cells using versatile all-in-one piggyBac transposons. *Methods Mol. Biol.* **1357**, 111–131 (2016).
79. J. In *et al.*, Enterohemorrhagic Escherichia coli reduce mucus and intermicrovillar bridges in human stem cell-derived colonoids. *Cell Mol. Gastroenterol. Hepatol.* **2**, 48–62.e3 (2016).
80. E. Oguro-Igashira *et al.*, The pyruvate–GPR31 axis promotes transepithelial dendrite formation in human intestinal dendritic cells. Gene Expression Omnibus. https://www.ncbi.nlm.nih.gov/geo/query/acc.cgi?acc=GSE240900. Deposited 15 August 2023.
81. E. Oguro-Igashira *et al.*, The pyruvate–GPR31 axis promotes transepithelial dendrite formation in human intestinal dendritic cells. Gene Expression Omnibus. https://www.ncbi.nlm.nih.gov/geo/query/acc.cgi?acc=GSE242091. Deposited 31 August 2023.
82. E. Oguro-Igashira *et al.*, The pyruvate–GPR31 axis promotes transepithelial dendrite formation in human intestinal dendritic cells. Gene Expression Omnibus. https://www.ncbi.nlm.nih.gov/geo/query/acc.cgi?acc=GSE272657. Deposited 19 July 2024.
83. E. Oguro-Igashira *et al.*, The pyruvate–GPR31 axis promotes transepithelial dendrite formation in human intestinal dendritic cells. Gene Expression Omnibus. https://www.ncbi.nlm.nih.gov/geo/query/acc.cgi?acc=GSE240895. Deposited 15 August 2023.